

# Arrangement of nearby minima and saddles in the mixed spherical energy landscapes

Jaron Kent-Dobias

Istituto Nazionale di Fisica Nucleare, Sezione di Roma I

July 18, 2023

## Abstract

The mixed spherical models were recently found to violate long-held assumptions about mean-field glassy dynamics. In particular, the threshold energy, where most stationary points are marginal and which in the simpler pure models attracts long-time dynamics, seems to lose significance. Here, we compute the typical distribution of stationary points relative to each other in mixed models with a replica symmetric complexity. We examine the stability of nearby points, accounting for the presence of an isolated eigenvalue in their spectrum due to their proximity. Despite finding rich structure not present in the pure models, we find nothing that distinguishes the points that do attract the dynamics. Instead, we find new geometric significance of the old threshold energy, and invalidate pictures of the arrangement of most marginal inherent states into a continuous manifold.

## Contents

<b>1</b>	<b>Introduction</b>	<b>2</b>
<b>2</b>	<b>Model</b>	<b>3</b>
<b>3</b>	<b>Results</b>	<b>6</b>
3.1	Barriers around deep states	6
3.2	Geometry of marginal states	7
<b>4</b>	<b>Calculation of the two-point complexity</b>	<b>10</b>
4.1	The Hessian factors	10
4.2	The other factors	11
4.3	Hubbard–Stratonovich	11
4.4	Saddle point	12
4.5	Expansion in the near neighborhood	14
<b>5</b>	<b>Isolated eigenvalue</b>	<b>16</b>
<b>6</b>	<b>Franz–Parisi potential</b>	<b>21</b>
<b>7</b>	<b>Conclusion</b>	<b>23</b>
	<b>References</b>	<b>24</b>

# 1 Introduction

Many systems exhibit “glassiness,” characterized by rapid slowing of dynamics over a short parameter interval. These include actual (structural) glasses, spin glasses, certain inference and optimization problems, and more. Glassiness is qualitatively understood to arise from structure of an energy or cost landscape, whether due to the proliferation of metastable states, or to the raising of barriers which cause effective dynamic constraints [1–3]. However, in most models there is no known quantitative correspondence between these landscape properties and the dynamic behavior they are purported to describe.

There is such a correspondence in one of the simplest mean-field model of glasses: in the pure spherical models, the dynamic transition corresponds with the energy level at which thermodynamic states attached to marginal inherent states<sup>1</sup> dominate the free energy [4]. At that level, called the *threshold energy*  $E_{\text{th}}$ , slices of the landscape at fixed energy undergo a percolation transition. In fact, this threshold energy is significant in other ways: it attracts the long-time dynamics after quenches in temperature to below the dynamical transition from any starting temperature [5, 6]. All of this can be understood in terms of the landscape structure.

In slightly less simple models, the mixed spherical models, the story changes. There are now a range of energies with exponentially many marginal minima. It was believed that the energy level at which these marginal minima are the most common type of stationary point would play the same role as the threshold energy in the pure models (in fact we will refer to this energy level as the threshold energy in the mixed models). However, recent work has shown that this is incorrect. Quenches from different starting temperatures above the dynamical transition temperature result in dynamics that approach different energy levels, and the purported threshold does not attract the long-time dynamics in most cases [7, 8].

This paper studies the two-point structure of stationary points in the mixed spherical models, or their arrangement relative to each other, previously studied only for the pure models [9]. This gives various kinds of information. When one point is a minimum, we see what other kinds of minima are nearby, and what kind of saddle points (barriers) separate them. When both points are saddles, we see the arrangement of barriers relative to each other, perhaps learning something about the geometry of the basins of attraction that they surround.

More specifically, one *reference* point is fixed with certain properties. Then, we compute the logarithm of the number of other points constrained to lie at a fixed overlap from the reference point. The fact of constraining the count to a fixed overlap produces constrained points with atypical properties. For instance, we will see that when the constrained overlap is made sufficiently large, the constrained points tend to have an isolated eigenvalue pulled out of their spectrum, and the associated eigenvector is correlated with the direction of the reference point. Without the proximity constraint, such an isolated eigenvalue amounts to a large deviation from the typical spectrum of stationary points.

In order to address the open problem of what attracts the long-time dynamics, we focus on the neighborhoods of the marginal minima, to see if there is anything interesting to differentiate sets of them from each other. Though we find rich structure in this population, their properties pivot around the debunked threshold energy, and the apparent attractors of long-time dynamics are not distinguished by this measure. Moreover, we show that the usual picture of a marginal ‘manifold’ of inherent states separated by subextensive barriers [10] is only true at the threshold energy, while at other energies typical marginal minima are far apart and separated by extensive barriers. Therefore, with respect to the problem of dynamics this paper merely deepens the outstanding issues.

In §2, we introduce the mixed spherical models and discuss their properties, defining many

---

<sup>1</sup>For this paper, which focuses on minima, we will take *state* to mean *minimum* or equivalently *inherent state* and not a thermodynamic state. Any discussion of thermodynamic or equilibrium states will explicitly specify this.

of the symbols and concepts relied on in the rest of the paper. In §3, we share the main results of the paper, with a large discussion of the neighborhood of marginal states. In §4 we detail the calculation of the two-point complexity, and in §5 and §6 we do the same for the properties of an isolated eigenvalue and for the zero-temperature Franz–Parisi potential. Finally in §7 we draw some conclusions from the study.

## 2 Model

The mixed spherical models are defined by the Hamiltonian

$$H(\mathbf{s}) = - \sum_p \frac{1}{p!} \sum_{i_1 \dots i_p}^N J_{i_1 \dots i_p}^{(p)} s_{i_1} \dots s_{i_p} \quad (1)$$

where the vectors  $\mathbf{s} \in \mathbb{R}^N$  are confined to the sphere  $\|\mathbf{s}\|^2 = N$  [11–13]. The coupling coefficients  $J$  are fully-connected and random, with zero mean and variance  $\overline{(J^{(p)})^2} = a_p p! / 2N^{p-1}$  scaled so that the energy is typically extensive. The overbar denotes an average over the coefficients  $J$ . The factors  $a_p$  in the variances are freely chosen constants that define the particular model. For instance, the ‘pure’  $p$ -spin model has  $a_{p'} = \delta_{p'p}$ . This class of models encompasses all statistically isotropic Gaussian random Hamiltonians defined on the hypersphere.

The covariance between the energy at two different points is a function of the overlap, or dot product, between those points, or

$$\overline{H(\mathbf{s}_1)H(\mathbf{s}_2)} = N f\left(\frac{\mathbf{s}_1 \cdot \mathbf{s}_2}{N}\right) \quad (2)$$

where the function  $f$  is defined from the coefficients  $a_p$  by

$$f(q) = \frac{1}{2} \sum_p a_p q^p \quad (3)$$

In this paper, we will focus on models with a replica symmetric complexity, but many of the intermediate formulae are valid for arbitrary replica symmetry breakings. At most 1RSB in the equilibrium is guaranteed if the function  $\chi(q) = f''(q)^{-1/2}$  is convex [12]. The complexity at the ground state must reflect the structure of equilibrium, and therefore be replica symmetric. We are not aware of any result guaranteeing this for the complexity away from the ground state, but we check that our replica-symmetric solutions satisfy the saddle point equations at 1RSB.

To enforce the spherical constraint at stationary points, we make use of a Lagrange multiplier  $\omega$ . This results in the extremal problem

$$H(\mathbf{s}) + \frac{\omega}{2} (\|\mathbf{s}\|^2 - N) \quad (4)$$

The gradient and Hessian at a stationary point are then

$$\nabla H(\mathbf{s}, \omega) = \partial H(\mathbf{s}) + \omega \mathbf{s} \quad \text{Hess } H(\mathbf{s}, \omega) = \partial \partial H(\mathbf{s}) + \omega I \quad (5)$$

where  $\partial = \frac{\partial}{\partial \mathbf{s}}$  denotes the derivative with respect to  $\mathbf{s}$ .

When we count stationary points, we classify them by certain properties. One of these is the energy density  $E = H/N$ . We will also fix the *stability*  $\mu = \frac{1}{N} \text{Tr Hess } H$ , also known as the radial reaction. In the mixed spherical models, all stationary points have a semicircle law for the eigenvalue spectrum of their Hessians, each with the same width  $\mu_m$ , but whose center is shifted by different amounts. Fixing the stability  $\mu$  fixes this shift, and therefore fixes the spectrum of

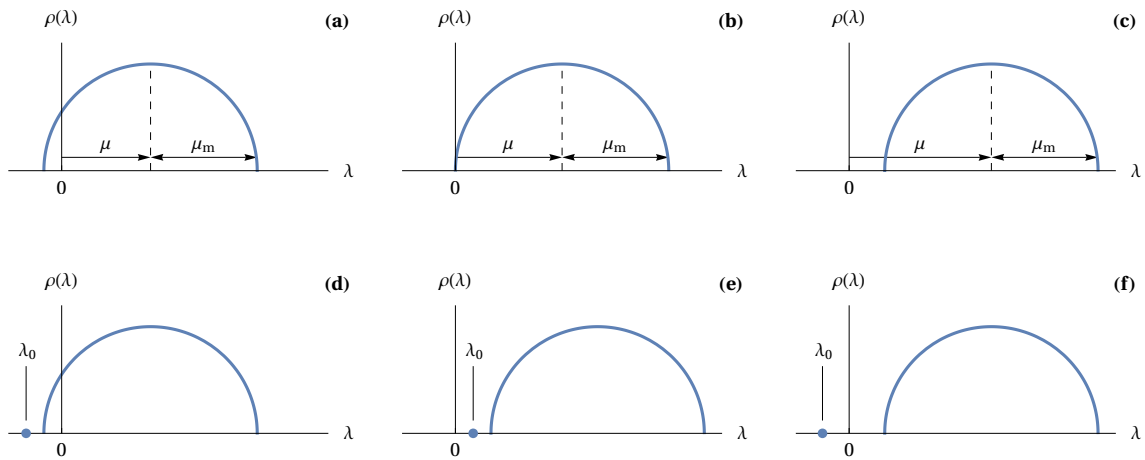


Figure 1: Illustration of the interpretation of the stability  $\mu$ , which sets the location of the center of the eigenvalue spectrum. In the top row we have spectra without an isolated eigenvalue. **(a)**  $\mu < \mu_m$ , there are an extensive number of downward directions, and the associated point is an *extensive saddle*. **(b)**  $\mu = \mu_m$  and we have a *marginal minimum* with asymptotically flat directions. **(c)**  $\mu > \mu_m$ , all eigenvalues are positive, and the point is a *stable minimum*. On the bottom we show what happens in the presence of an isolated eigenvalue. **(d)** One eigenvalue leaves the bulk spectrum of a saddle point and it remains a saddle point, but now with an eigenvector correlated with the orientation of the reference vector, so we call this a *oriented saddle*. **(e)** The same happens for a minimum, and we can call it an *oriented minimum*. **(f)** One eigenvalue outside a positive bulk spectrum is negative, destabilizing what would otherwise have been a stable minimum, producing an *oriented index-one saddle*.

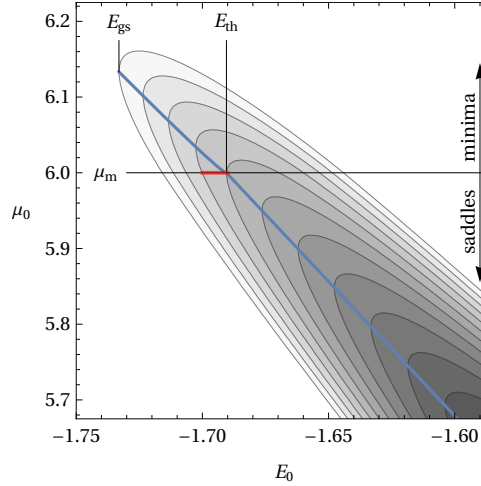


Figure 2: Plot of the complexity (logarithm of the number of stationary points) for the 3 + 4 mixed spherical model studied in this paper. Energies and stabilities of interest are marked, including the ground state energy and stability  $E_{gs}$ , the marginal stability  $\mu_m$ , and the threshold energy  $E_{th}$ . The blue line shows the location of the most common type of stationary point at each energy level. The highlighted red region shows the approximate range of minima which attract aging dynamics from a quench to zero temperature found in [7].

the associated stationary point. When the stability is smaller than the width of the spectrum, or  $\mu < \mu_m$ , there are an extensive number of negative eigenvalues, and the stationary point is a saddle with a large index whose value is set by the stability. When the stability is greater than the width of the spectrum, or  $\mu > \mu_m$ , the semicircle distribution lies only over positive eigenvalues, and unless an isolated eigenvalue leaves the semicircle and becomes negative, the stationary point is a minimum. Finally, when  $\mu = \mu_m$ , the edge of the semicircle touches zero and we have marginal minima. Fig. 1 shows what different values of the stability imply about the spectrum at stationary points.

In the pure spherical models,  $E$  and  $\mu$  cannot be fixed separately: fixing one uniquely fixes the other. This property leads to the great simplification of these models: marginal minima exist *only* at one energy level, and therefore only that energy has the possibility of trapping the long-time dynamics. In generic mixed models this is not the case and at a given energy level  $E$  there are many stabilities for which exponentially many stationary points are found. We define the threshold energy  $E_{th}$  as the energy at which most stationary points are marginal. Note that crucially this is *not* the energy that has the most marginal stationary points: this energy level with the largest number of marginal points has even more saddles of extensive index. So  $E_{th}$  contains a *minority* of the marginal points, even if those marginal points are the *majority* of stationary points with energy  $E_{th}$ .

In this study, we focus exclusively on the model studied in [7], whose covariance function is given by

$$f_{3+4}(q) = \frac{1}{2}(q^3 + q^4) \quad (6)$$

First, it has convex  $f''(q)^{-1/2}$ , so at least the ground state complexity must be replica symmetric, as in the pure spherical models. Second, properties of its long-time dynamics have been extensively studied. The annealed one-point complexity of these models was calculated in [14], and for this model the annealed is expected to be correct. The complexity of this model is plotted in Fig. 2.

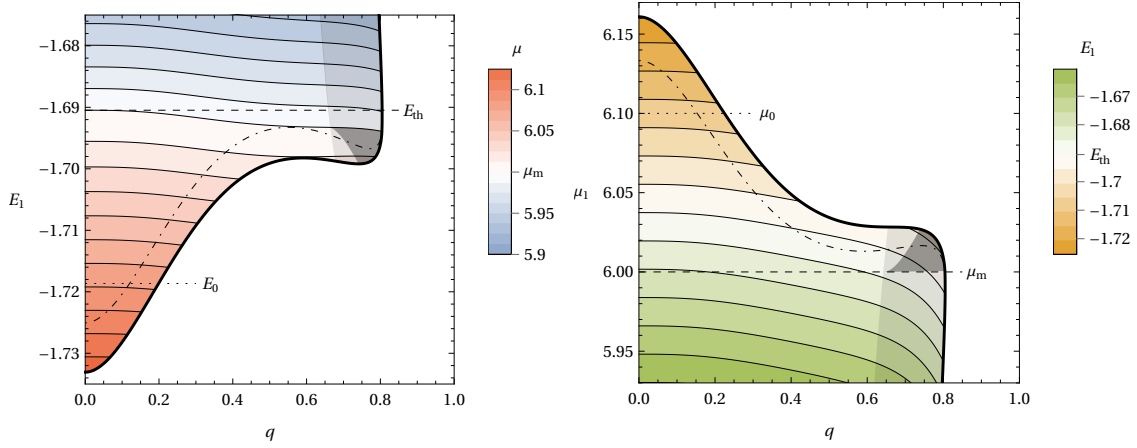


Figure 3: The neighborhood of a reference minimum with  $E_0 = -1.71865 < E_{\text{th}}$  and  $\mu_0 = 6.1 > \mu_m$ . **Left:** The most common type of stationary point lying at fixed overlap  $q$  and energy  $E_1$  from the reference minimum. The black line gives the smallest or largest energies where neighbors can be found at a given overlap. **Right:** The most common type of stationary point lying at fixed overlap  $q$  and stability  $\mu_1$  from the reference minimum. Note that this describes a different set of stationary points than shown in the left plot. On both plots, the shading of the righthand part depicts the state of an isolated eigenvalue in the spectrum of the Hessian of the neighboring points. Those more lightly shaded are points with an isolated eigenvalue that does not change their stability, e.g., corresponding with Fig. 1(d-e). The more darkly shaded are oriented index-one saddles, e.g., corresponding with Fig. 1(f). The dot-dashed lines on both plots depict the trajectory of the solid line on the other plot. In this case, the points lying nearest to the reference minimum are saddles with  $\mu < \mu_m$ , but with energies smaller than the threshold energy.

### 3 Results

Our results are in the form of the two-point complexity, which is defined as the logarithm of the number of stationary points with energy  $E_1$  and stability  $\mu_1$  that lie at an overlap  $q$  with a typical reference stationary point whose energy is  $E_0$  and stability is  $\mu_0$ . When the complexity is positive, there are exponentially many stationary points with the given properties conditioned on the existence of the reference one. When it is zero, there are only order-one such points, and when it is negative there are exponentially few (effectively, none). In the examples below, the boundary of zero complexity between exponentially many and few points is often highlighted. Finally, as a result of the condition that the counted points lie with a given proximity to the reference point, their spectrum can be modified by the presence of an isolated eigenvalue, which can change the stability as in Fig. 1.

#### 3.1 Barriers around deep states

If the reference configuration is restricted to stable minima, then there is a gap in the overlap between those minima and their nearest neighbors in configuration space. We can characterize these neighbors as a function of their overlap and stability, with one example seen in Fig. 3. For stable minima, the qualitative results for the pure  $p$ -spin model continue to hold, with some small modifications [9].

First, the nearest neighbor points are always oriented saddles, sometimes saddles with an extensive index and sometimes index-one saddles (Fig. 1(d, f)). Like in the pure models, the emergence of oriented index-one saddles along the line of lowest-energy states at a given overlap

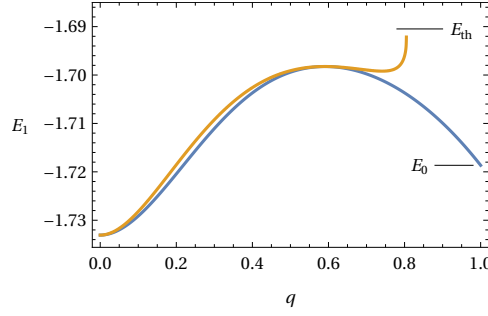


Figure 4: Comparison of the lowest-energy stationary points at overlap  $q$  with a reference minimum of  $E_0 = -1.71865 < E_{\text{th}}$  and  $\mu_0 = 6.1 > \mu_m$  (yellow, top), and the zero-temperature Franz–Parisi potential with respect to the same reference minimum (blue, bottom). The two curves coincide precisely at their minimum  $q = 0$  and at the local maximum  $q \approx 0.5909$ .

occurs at the local minimum of this line. Unlike the pure models, neighbors exist for independent  $\mu_1$  and  $E_1$ , and the line of lowest-energy states at a given overlap is different from the line of maximally-stable states at a given overlap.

Also like the pure models, there is a correspondence between the maximum of the zero-temperature Franz–Parisi potential restricted to minima of the specified type and the local maximum of the neighbor complexity along the line of lowest-energy states. This is seen in Fig. 4.

### 3.2 Geometry of marginal states

The set of marginal states is of special interest. First, it has more structure than in the pure models, with different types of marginal states being found at different energies. Second, these states attract the dynamics (as evidenced by power-law relaxations), and so are the inevitable end-point of equilibrium and algorithmic processes [15]. We find, surprisingly, that the properties of marginal states pivot around the threshold energy, the energy at which most stationary points are marginal.

- **Energies below the threshold.** Marginal states have a macroscopic gap in their overlap with nearby minima and saddles. The nearest stationary points are saddles with an oriented direction, and always have a higher energy density than the reference state. Fig. 5 shows examples of the neighborhoods of these marginal minima.
- **Energies above the threshold.** Marginal states have neighboring stationary points at arbitrarily close distance, with a quadratic pseudogap in their complexity. The nearest ones are *strictly* saddle points with an extensive number of downward directions and always have a higher energy density than the reference state. The nearest neighboring marginal states have an overlap gap with the reference state. Fig. 6 shows examples of the neighborhoods of these marginal minima.
- **At the threshold energy.** Marginal states have neighboring stationary points at arbitrarily close distance, with a cubic pseudogap in their complexity. The nearest ones include oriented saddle points with an extensive number of downward directions, and oriented stable and marginal minima. Though most of the nearest states are found at higher energies, they can be found at the same energy density as the reference state. Fig. 7 shows examples of the neighborhoods of these marginal states.

This leads us to some general conclusions. First, at all energy densities except at the threshold energy, *typical marginal minima are separated by extensive energy barriers*. Therefore, the

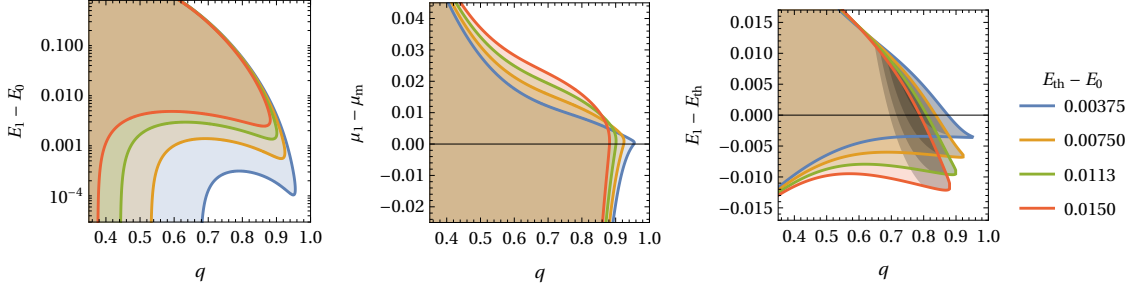


Figure 5: The neighborhood of marginal states at several energies below the threshold energy. **Left:** The range of energies  $E_1$  at which nearby states are found. For any  $E_0 < E_{\text{th}}$ , the nearest class of states is at an extensive distance, and their energies are higher than that of the reference configuration. **Center:** The range of stabilities  $\mu_1$  at which nearby states are found. For  $E_0$  near the threshold, the nearest states are always index-one saddles with  $\mu > \mu_m$ , but as the overlap gap widens their population becomes model-dependent. **Right:** The range of energies at which *other* marginal states are found. Here, the more darkly shaded regions denote where an isolated eigenvalue appears. Marginal states below the threshold are always separated by a gap in their overlap.

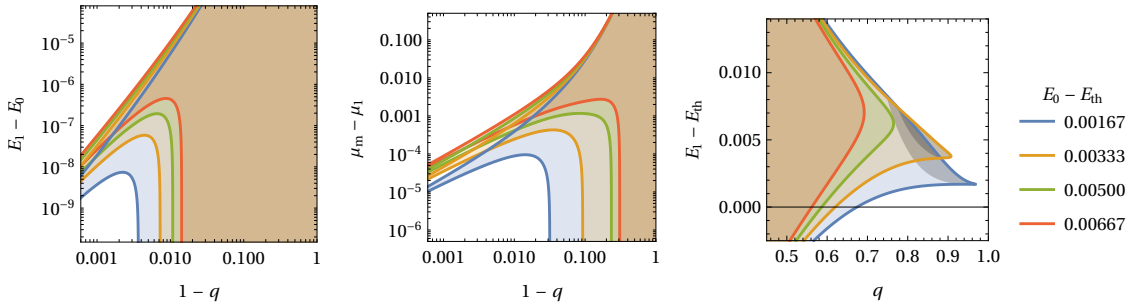


Figure 6: The neighborhood of marginal states at several energies above the threshold energy. **Left:** The range of energies  $E_1$  at which nearby states are found. For any  $E_0 > E_{\text{th}}$ , there always exists a  $q$  sufficiently close to one such that the nearby states have strictly greater energy than the reference state. **Center:** The range of stabilities  $\mu_1$  at which nearby states are found. There is always a sufficiently large overlap beyond which all nearby states are saddle with an extensive number of downward directions. **Right:** The range of energies at which *other* marginal states are found. Here, the more darkly shaded regions denote where an isolated eigenvalue appears. Marginal states above the threshold are always separated by a gap in their overlap.



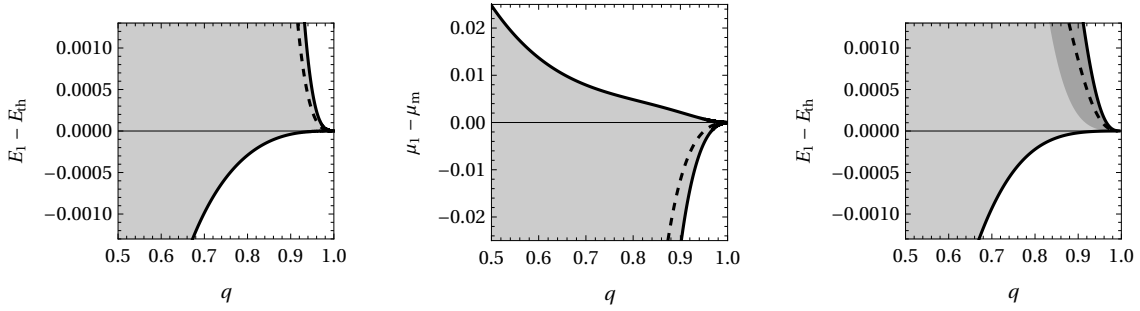


Figure 7: The neighborhood of marginal minima at the threshold energy  $E_0 = E_{\text{th}}$ . In all plots, the dashed lines show the population of most common neighbors at the given overlap  $q$ . **Left:** The range of energies  $E_1$  at which nearby points are found. The approach of both the minimum and maximum energies goes like  $(1 - q)^3$ . **Center:** The range of stabilities  $\mu_1$  at which nearby points are found. The approach of both limits goes like  $(1 - q)^2$ . **Right:** The range of nearby marginal minima. The more darkly shaded region denotes where an isolated eigenvalue appears. Marginal minima at the threshold lie asymptotically close together.

picture of a marginal *manifold* of many (even all) marginal states lying arbitrarily close and being connected by subextensive energy barriers can only describe the collection of marginal minima at the threshold energy, or an atypical population of marginal minima. At energies both below and above the threshold energy, typical marginal minima are isolated from each other.

We must put a small caveat here: in *any* situation, this calculation admits order-one other marginal minima to lie a subextensive distance from the reference point. For such a population of points,  $\Sigma_{12} = 0$  and  $q = 1$ , which is always a permitted solution when at least one marginal direction exists. These points are separated by small barriers from one another, but they also cover a vanishing piece of configuration space, and each such cluster of points is isolated by extensive barriers from each other cluster in the way described above. To move on a ‘manifold’ of nearby marginal minima within such a cluster cannot describe aging, since the overlap with the initial condition will never change from one.

This has implications for how quench dynamics should be interpreted. When typical marginal states are approached above the threshold energy, they must have been via the neighborhood of saddles with an extensive index, not other marginal states. On the other hand, typical marginal states approached below the threshold energy must be reached after an extensive distance in configuration space without encountering any stationary point. The geometric conditions of the neighborhoods above and below are quite different, but the observed aging dynamics don’t appear to qualitatively change [7, 8]. Therefore, if the marginal minima attracting dynamics are typical, the conditions in the neighborhood of the marginal minimum eventually reached at infinite time appear to be irrelevant for the nature of aging dynamics at any finite time.

A version of this story was told a long time ago by the authors of [10], who write on aging in the pure spherical models where the limit of  $N \rightarrow \infty$  is taken before that of  $t \rightarrow \infty$ : “it is important to remark that this [...] does *not* mean that the system relaxes into a near-threshold state: at all finite times an infinite system has a Hessian with an *infinite* number of directions in which the energy is a maximum. [...] We have seen that the saddles separating threshold minima are typically  $O(N^{1/3})$  above the threshold level, while the energy is at all finite times  $O(N)$  above this level.” In the present case of the mixed spherical models, where [7] has shown aging dynamics asymptotically approaching marginal states that we have shown have  $O(N)$  saddles separating them, this lesson must be taken all the more seriously.

On the other hand, it is possible that *atypical* marginal minima are relevant for attracting the dynamics. Studying these points would require a different kind of computation, where the fixed

reference point is abandoned and both points are treated on equal footing. Such a calculation is beyond the scope of this paper, but is clear fodder for future research.

## 4 Calculation of the two-point complexity

We introduce the Kac–Rice [16, 17] measure

$$d\nu_H(\mathbf{s}, \omega) = 2 d\mathbf{s} d\omega \delta(\|\mathbf{s}\|^2 - N) \delta(\nabla H(\mathbf{s}, \omega)) |\det \text{Hess } H(\mathbf{s}, \omega)| \quad (7)$$

which counts stationary points of the function  $H$ . If integrated over configuration space,  $\mathcal{N}_H = \int d\nu_H(\mathbf{s}, \omega)$  gives the total number of stationary points in the function. The Kac–Rice method has been used by in many studies to analyze the geometry of random functions [18–20]. More interesting is the measure conditioned on the energy density  $E$  and stability  $\mu$  of the points,

$$d\nu_H(\mathbf{s}, \omega | E, \mu) = d\nu_H(\mathbf{s}, \omega) \delta(NE - H(\mathbf{s})) \delta(N\mu - \text{Tr Hess } H(\mathbf{s}, \omega)) \quad (8)$$

While  $\mu$  is strictly the trace of the Hessian, we call it the stability because in this family of models all stationary points have a bulk spectrum of the same shape, shifted by different constants. The stability  $\mu$  sets this shift, and therefore determines if the spectrum has bulk support on zero. See Fig. 1 for examples.

We want the typical number of stationary points with energy density  $E_1$  and stability  $\mu_1$  that lie a fixed overlap  $q$  from a reference stationary point of energy density  $E_0$  and stability  $\mu_0$ . For a *typical* number, we cannot average the total number  $\mathcal{N}_H$ , which is exponentially large in  $N$  and therefore can be biased by atypical examples. Therefore, we will average the logarithm of this number. The two-point complexity is therefore defined by

$$\Sigma_{12} = \frac{1}{N} \int \frac{d\nu_H(\boldsymbol{\sigma}, \varsigma | E_0, \mu_0)}{\int d\nu_H(\boldsymbol{\sigma}', \varsigma' | E_0, \mu_0)} \log \left( \int d\nu_H(\mathbf{s}, \omega | E_1, \mu_1) \delta(Nq - \boldsymbol{\sigma} \cdot \mathbf{s}) \right) \quad (9)$$

Both the denominator and the logarithm are treated using the replica trick, which yields

$$\Sigma_{12} = \frac{1}{N} \lim_{n \rightarrow 0} \lim_{m \rightarrow 0} \frac{\partial}{\partial n} \int \left( \prod_{b=1}^m d\nu_H(\boldsymbol{\sigma}_b, \varsigma_b | E_0, \mu_0) \right) \left( \prod_{a=1}^n d\nu_H(\mathbf{s}_a, \omega_a | E_1, \mu_1) \delta(Nq - \boldsymbol{\sigma}_1 \cdot \mathbf{s}_a) \right) \quad (10)$$

Note that because of the structure of (9),  $\boldsymbol{\sigma}_1$  is special among the set of  $\boldsymbol{\sigma}$  replicas, since it alone is constrained to lie a given overlap from the  $\mathbf{s}$  replicas. This replica asymmetry will be important later.

### 4.1 The Hessian factors

The double partial derivatives of the energy are Gaussian with the variance

$$\overline{(\partial_i \partial_j H(\mathbf{s}))^2} = \frac{1}{N} f''(1) \quad (11)$$

which means that the matrix of partial derivatives belongs to the GOE class. Its spectrum is given by the Wigner semicircle

$$\rho(\lambda) = \begin{cases} \frac{2}{\pi} \sqrt{1 - \left(\frac{\lambda}{\mu_m}\right)^2} & \lambda^2 \leq \mu_m^2 \\ 0 & \text{otherwise} \end{cases} \quad (12)$$

with radius  $\mu_m = \sqrt{4f''(1)}$ . Since the Hessian differs from the matrix of partial derivatives by adding the constant diagonal matrix  $\omega I$ , it follows that the spectrum of the Hessian is a Wigner semicircle shifted by  $\omega$ , or  $\rho(\lambda + \omega)$ .

The average over factors depending on the Hessian alone can be made separately from those depending on the gradient or energy, since for random Gaussian fields the Hessian is independent of these [20]. In principle the fact that we have conditioned the Hessian to belong to stationary points of certain energy, stability, and proximity to another stationary point will modify its statistics, but these changes will only appear at subleading order in  $N$  [9]. At leading order, the various expectations factorize, each yielding

$$\overline{|\det \text{Hess } H(\mathbf{s}, \omega)| \delta(N\mu - \text{Tr Hess } H(\mathbf{s}, \omega))} = e^{N \int d\lambda \rho(\lambda + \mu) \log |\lambda|} \delta(N\mu - N\omega) \quad (13)$$

Therefore, all of the Lagrange multipliers are fixed to the stabilities  $\mu$ . We define the function

$$\begin{aligned} \mathcal{D}(\mu) &= \int d\lambda \rho(\lambda + \mu) \log |\lambda| \\ &= \begin{cases} \frac{1}{2} + \log\left(\frac{1}{2}\mu_m\right) + \frac{\mu^2}{\mu_m^2} & \mu^2 \leq \mu_m^2 \\ \frac{1}{2} + \log\left(\frac{1}{2}\mu_m\right) + \frac{\mu^2}{\mu_m^2} - \left|\frac{\mu}{\mu_m}\right| \sqrt{\left(\frac{\mu}{\mu_m}\right)^2 - 1} - \log\left(\left|\frac{\mu}{\mu_m}\right| - \sqrt{\left(\frac{\mu}{\mu_m}\right)^2 - 1}\right) & \mu^2 > \mu_m^2 \end{cases} \end{aligned} \quad (14)$$

and the full factor due to the Hessians is

$$e^{Nm\mathcal{D}(\mu_0) + Nn\mathcal{D}(\mu_1)} \left[ \prod_a^m \delta(N\mu_0 - N\zeta_a) \right] \left[ \prod_a^n \delta(N\mu_1 - N\omega_a) \right] \quad (15)$$

## 4.2 The other factors

Having integrated over the Lagrange multipliers using the  $\delta$ -functions resulting from the average of the Hessians, any  $\delta$ -functions in the remaining integrand we Fourier transform into their integral representation over auxiliary fields. The resulting integrand has the form

$$e^{Nm\hat{\beta}_0 E_0 + Nn\hat{\beta}_1 E_1 - \sum_a^m [(\boldsymbol{\sigma}_a \cdot \hat{\boldsymbol{\sigma}}_a) \mu_0 - \frac{1}{2} \hat{\mu}_0 (N - \boldsymbol{\sigma}_a \cdot \boldsymbol{\sigma}_a)] - \sum_a^n [(s_a \cdot \hat{s}_a) \mu_1 - \frac{1}{2} \hat{\mu}_1 (N - s_a \cdot s_a) - \frac{1}{2} \hat{\mu}_{12} (Nq - \boldsymbol{\sigma}_1 \cdot s_a)]} + \int dt O(\mathbf{t}) H(\mathbf{t}) \quad (16)$$

where we have introduced the linear operator

$$O(\mathbf{t}) = \sum_a^m \delta(\mathbf{t} - \boldsymbol{\sigma}_a) (i\hat{\boldsymbol{\sigma}}_a \cdot \partial_{\mathbf{t}} - \hat{\beta}_0) + \sum_a^n \delta(\mathbf{t} - s_a) (i\hat{s}_a \cdot \partial_{\mathbf{t}} - \hat{\beta}_1) \quad (17)$$

Here the  $\hat{\beta}$ s are the fields auxiliary to the energy constraints, the  $\hat{\mu}$ s are auxiliary to the spherical and overlap constraints, and the  $\hat{\boldsymbol{\sigma}}$ s and  $\hat{s}$ s are auxiliary to the constraint that the gradient be zero. We have written the  $H$ -dependent terms in this strange form for the ease of taking the average over  $H$ : since it is Gaussian-correlated, it follows that

$$\overline{e^{\int dt O(\mathbf{t}) H(\mathbf{t})}} = e^{\frac{1}{2} \int dt dt' O(\mathbf{t}) O(\mathbf{t}') \overline{H(\mathbf{t}) H(\mathbf{t}')}} = e^{N \frac{1}{2} \int dt dt' O(\mathbf{t}) O(\mathbf{t}') f\left(\frac{\mathbf{t}\mathbf{t}'}{N}\right)} \quad (18)$$

It remains only to apply the doubled operators to  $f$  and then evaluate the simple integrals over the  $\delta$  measures. We do not include these details, which are standard.

## 4.3 Hubbard–Stratonovich

Having expanded this expression, we are left with an argument in the exponential which is a function of scalar products between the fields  $\mathbf{s}$ ,  $\hat{s}$ ,  $\boldsymbol{\sigma}$ , and  $\hat{\boldsymbol{\sigma}}$ . We will change integration coordinates from these fields to matrix fields given by their scalar products, defined as

$$\begin{aligned} C_{ab}^{00} &= \frac{1}{N} \boldsymbol{\sigma}_a \cdot \boldsymbol{\sigma}_b & R_{ab}^{00} &= -i \frac{1}{N} \boldsymbol{\sigma}_a \cdot \hat{\boldsymbol{\sigma}}_b & D_{ab}^{00} &= \frac{1}{N} \hat{\boldsymbol{\sigma}}_a \cdot \hat{\boldsymbol{\sigma}}_b \\ C_{ab}^{01} &= \frac{1}{N} \boldsymbol{\sigma}_a \cdot s_b & R_{ab}^{01} &= -i \frac{1}{N} \boldsymbol{\sigma}_a \cdot \hat{s}_b & R_{ab}^{10} &= -i \frac{1}{N} \hat{\boldsymbol{\sigma}}_a \cdot s_b & D_{ab}^{01} &= \frac{1}{N} \hat{\boldsymbol{\sigma}}_a \cdot \hat{s}_b \\ C_{ab}^{11} &= \frac{1}{N} s_a \cdot s_b & R_{ab}^{11} &= -i \frac{1}{N} s_a \cdot \hat{s}_b & D_{ab}^{11} &= \frac{1}{N} \hat{s}_a \cdot \hat{s}_b \end{aligned} \quad (19)$$

We insert into the integral the product of  $\delta$ -functions enforcing these definitions, integrated over the new matrix fields, which is equivalent to multiplying by one. Once this is done, the many scalar products appearing throughout can be replaced by the matrix fields, and the original vector fields can be integrated over. Conjugate matrix field integrals created when the  $\delta$ -functions are promoted to exponentials can be evaluated by saddle point in the standard way, yielding an effective action depending on the above matrix fields alone.

#### 4.4 Saddle point

We will always assume that the square matrices  $C^{00}$ ,  $R^{00}$ ,  $D^{00}$ ,  $C^{11}$ ,  $R^{11}$ , and  $D^{11}$  are hierarchical matrices, with each set of three sharing the same hierarchical structure. In particular, we immediately define  $c_d^{00}$ ,  $r_d^{00}$ ,  $d_d^{00}$ ,  $c_d^{11}$ ,  $r_d^{11}$ , and  $d_d^{11}$  as the value of the diagonal elements of these matrices, respectively. Note that  $c_d^{00} = c_d^{11} = 1$  due to the spherical constraint.

Defining the ‘block’ fields  $\mathcal{Q}_{00} = (\hat{\beta}_0, \hat{\mu}_0, C^{00}, R^{00}, D^{00})$ ,  $\mathcal{Q}_{11} = (\hat{\beta}_1, \hat{\mu}_1, C^{11}, R^{11}, D^{11})$ , and  $\mathcal{Q}_{01} = (\hat{\mu}_{01}, C^{01}, R^{01}, R^{10}, D^{01})$  the resulting complexity is

$$\Sigma_{01} = \frac{1}{N} \lim_{n \rightarrow 0} \lim_{m \rightarrow 0} \frac{\partial}{\partial n} \int d\mathcal{Q}_{00} d\mathcal{Q}_{11} d\mathcal{Q}_{01} e^{Nm\mathcal{S}_0(\mathcal{Q}_{00}) + Nn\mathcal{S}_1(\mathcal{Q}_{11}, \mathcal{Q}_{01} | \mathcal{Q}_{00})} \quad (20)$$

where

$$\begin{aligned} \mathcal{S}_0(\mathcal{Q}_{00}) &= \hat{\beta}_0 E_0 - r_d^{00} \mu_0 - \frac{1}{2} \hat{\mu}_0 (1 - c_d^{00}) + \mathcal{D}(\mu_0) \\ &+ \frac{1}{m} \left\{ \frac{1}{2} \sum_{ab}^m [\hat{\beta}_1^2 f(C_{ab}^{00}) + (2\hat{\beta}_1 R_{ab}^{00} - D_{ab}^{00}) f'(C_{ab}^{00}) + (R_{ab}^{00})^2 f''(C_{ab}^{00})] + \frac{1}{2} \log \det \begin{bmatrix} C^{00} & R^{00} \\ R^{00} & D^{00} \end{bmatrix} \right\} \end{aligned} \quad (21)$$

is the action for the ordinary, one-point complexity, and remainder is given by

$$\begin{aligned} \mathcal{S}(\mathcal{Q}_{11}, \mathcal{Q}_{01} | \mathcal{Q}_{00}) &= \hat{\beta}_1 E_1 - r_d^{11} \mu_1 - \frac{1}{2} \hat{\mu}_1 (1 - c_d^{11}) + \mathcal{D}(\mu_1) \\ &+ \frac{1}{n} \sum_b^n \left\{ -\frac{1}{2} \hat{\mu}_{12} (q - C_{1b}^{01}) + \sum_a^m [\hat{\beta}_0 \hat{\beta}_1 f(C_{ab}^{01}) + (\hat{\beta}_0 R_{ab}^{01} + \hat{\beta}_1 R_{ab}^{10} - D_{ab}^{01}) f'(C_{ab}^{01}) + R_{ab}^{01} R_{ab}^{10} f''(C_{ab}^{01})] \right\} \\ &+ \frac{1}{n} \left\{ \frac{1}{2} \sum_{ab}^n [\hat{\beta}_1^2 f(C_{ab}^{11}) + (2\hat{\beta}_1 R_{ab}^{11} - D_{ab}^{11}) f'(C_{ab}^{11}) + (R_{ab}^{11})^2 f''(C_{ab}^{11})] \right. \\ &\left. + \frac{1}{2} \log \det \left( \begin{bmatrix} C^{11} & iR^{11} \\ iR^{11} & D^{11} \end{bmatrix} - \begin{bmatrix} C^{01} & iR^{01} \\ iR^{10} & D^{01} \end{bmatrix}^T \begin{bmatrix} C^{00} & iR^{00} \\ iR^{00} & D^{00} \end{bmatrix}^{-1} \begin{bmatrix} C^{01} & iR^{01} \\ iR^{10} & D^{01} \end{bmatrix} \right) \right\} \end{aligned} \quad (22)$$

Because of the structure of this problem in the twin limits of  $m$  and  $n$  to zero, the parameters  $\mathcal{Q}_{00}$  can be evaluated at a saddle point of  $\mathcal{S}_0$  alone. This means that these parameters will take the same value they take when the ordinary, 1-point complexity is calculated. For a replica symmetric complexity of the reference point, this results in

$$\hat{\beta}_0 = -\frac{\mu_0 f'(1) + E_0 (f'(1) + f''(1))}{u_f} \quad (23)$$

$$r_d^{00} = \frac{\mu_0 f(1) + E_0 f'(1)}{u_f} \quad (24)$$

$$d_d^{00} = \frac{1}{f'(1)} - \left( \frac{\mu_0 f(1) + E_0 f'(1)}{u_f} \right)^2 \quad (25)$$

where we define for brevity (here and elsewhere) the constants

$$u_f = f(1)(f'(1) + f''(1)) - f'(1)^2 \quad v_f = f'(1)(f''(1) + f'''(1)) - f''(1)^2 \quad (26)$$

Note that because the coefficients of  $f$  must be nonnegative for  $f$  to be a sensible covariance, both  $u_f$  and  $v_f$  are strictly positive. Note also that  $u_f = v_f = 0$  if  $f$  is a homogeneous polynomial as in the pure models. These expressions are invalid for the pure models because  $\mu_0$  and  $E_0$  cannot be fixed independently; we would have done the equivalent of inserting two identical  $\delta$ -functions. For the pure models, the terms  $\hat{\beta}_0$  and  $\hat{\beta}_1$  must be set to zero in our prior formulae (as if the energy was not constrained) and then the saddle point taken.

In general, we expect the  $m \times n$  matrices  $C^{01}$ ,  $R^{01}$ ,  $R^{10}$ , and  $D^{01}$  to have constant rows of length  $n$ , with blocks of rows corresponding to the RSB structure of the single-point complexity. For the scope of this paper, where we restrict ourselves to replica symmetric complexities, they have the following form at the saddle point:

$$C^{01} = \begin{array}{c} \leftarrow n \rightarrow \\ \begin{bmatrix} q & \cdots & q \\ 0 & \cdots & 0 \\ \vdots & \ddots & \vdots \\ 0 & \cdots & 0 \end{bmatrix} \\ \uparrow \\ m-1 \\ \downarrow \end{array} \quad R^{01} = \begin{bmatrix} r_{01} & \cdots & r_{01} \\ 0 & \cdots & 0 \\ \vdots & \ddots & \vdots \\ 0 & \cdots & 0 \end{bmatrix} \quad R^{10} = \begin{bmatrix} r_{10} & \cdots & r_{10} \\ 0 & \cdots & 0 \\ \vdots & \ddots & \vdots \\ 0 & \cdots & 0 \end{bmatrix} \quad D^{01} = \begin{bmatrix} d_{01} & \cdots & d_{01} \\ 0 & \cdots & 0 \\ \vdots & \ddots & \vdots \\ 0 & \cdots & 0 \end{bmatrix} \quad (27)$$

where only the first row is nonzero. The other entries, which correspond to the completely uncorrelated replicas in an RSB picture, are all zero because uncorrelated vectors on the sphere are orthogonal.

The inverse of block hierarchical matrix is still a block hierarchical matrix, since

$$\begin{bmatrix} C^{00} & iR^{00} \\ iR^{00} & D^{00} \end{bmatrix}^{-1} = \begin{bmatrix} (C^{00}D^{00} + R^{00}R^{00})^{-1}D^{00} & -i(C^{00}D^{00} + R^{00}R^{00})^{-1}R^{00} \\ -i(C^{00}D^{00} + R^{00}R^{00})^{-1}R^{00} & (C^{00}D^{00} + R^{00}R^{00})^{-1}C^{00} \end{bmatrix} \quad (28)$$

Because of the structure of the 01 matrices, the volume element will depend only on the diagonals of the matrices in this inverse block matrix. If we define

$$\tilde{c}_d^{00} = [(C^{00}D^{00} + R^{00}R^{00})^{-1}C^{00}]_d \quad (29)$$

$$\tilde{r}_d^{00} = [(C^{00}D^{00} + R^{00}R^{00})^{-1}R^{00}]_d \quad (30)$$

$$\tilde{d}_d^{00} = [(C^{00}D^{00} + R^{00}R^{00})^{-1}D^{00}]_d \quad (31)$$

as the diagonals of the blocks of the inverse matrix, then the result of the product is

$$\begin{bmatrix} C^{01} & iR^{01} \\ iR^{10} & D^{01} \end{bmatrix}^T \begin{bmatrix} C^{00} & iR^{00} \\ iR^{00} & D^{00} \end{bmatrix}^{-1} \begin{bmatrix} C^{01} & iR^{01} \\ iR^{10} & D^{01} \end{bmatrix} = \begin{bmatrix} q^2 \tilde{d}_d^{00} + 2qr_{10} \tilde{r}_d^{00} - r_{10}^2 \tilde{d}_d^{00} & i [d_{01}(r_{10} \tilde{c}_d^{00} - q \tilde{r}_d^{00}) + r_{01}(r_{10} \tilde{r}_d^{00} + q \tilde{d}_d^{00})] \\ i [d_{01}(r_{10} \tilde{c}_d^{00} - q \tilde{r}_d^{00}) + r_{01}(r_{10} \tilde{r}_d^{00} + q \tilde{d}_d^{00})] & d_{01}^2 \tilde{c}_d^{00} + 2r_{01}d_{01} \tilde{r}_d^{00} - r_{01}^2 \tilde{d}_d^{00} \end{bmatrix} \quad (32)$$

where each block is a constant  $n \times n$  matrix. Because the matrices  $C^{00}$ ,  $R^{00}$ , and  $D^{00}$  are diagonal in the replica symmetric case, the diagonals of the blocks above take a simple form:

$$\tilde{c}_d^{00} = f'(1) \quad \tilde{r}_d^{00} = r_d^{00} f'(1) \quad \tilde{d}_d^{00} = d_d^{00} f'(1) \quad (33)$$

Once these expressions are inserted into the complexity, the limits of  $n$  and  $m$  to zero can be taken, and the parameters from  $D^{01}$  and  $D^{11}$  can be extremized explicitly. The resulting expression for

the complexity, which must still be extremized over the parameters  $\hat{\beta}_1$ ,  $r^{01}$ ,  $r_d^{11}$ ,  $r_0^{11}$ , and  $q_0^{11}$ , is

$$\begin{aligned} \Sigma_{12}(E_0, \mu_0, E_1, \mu_1, q) = & \text{extremum}_{\hat{\beta}_1, r_d^{11}, r_0^{11}, r^{01}, q_0^{11}} \left\{ \mathcal{D}(\mu_1) - \frac{1}{2} + \hat{\beta}_1 E_1 - r_d^{11} \mu_1 + \hat{\beta}_1 (r_d^{11} f'(1) - r_0^{11} f'(q_0^{11})) \right. \\ & + \hat{\beta}_0 \hat{\beta}_1 f(q) + (\hat{\beta}_0 r^{01} + \hat{\beta}_1 r^{10} + r_d^{00} r^{01}) f'(q) + \frac{r_d^{11} - r_0^{11}}{1 - q_0^{11}} (r^{10} - q r_d^{00}) f'(q) \\ & + \frac{1}{2} \left[ \hat{\beta}_1^2 (f(1) - f(q_0^{11})) + (r_d^{11})^2 f''(1) + 2r^{01} r^{10} f''(q) - (r_0^{11})^2 f''(q_0^{11}) + \frac{(r^{10} - q r_d^{00})^2}{1 - q_0^{11}} f'(1) \right. \\ & + \frac{1 - q^2}{1 - q_0^{11}} + \left. \left( (r^{01})^2 - \frac{r_d^{11} - r_0^{11}}{1 - q_0^{11}} \left( 2q r^{01} - \frac{(1 - q^2) r_0^{11} - (q_0^{11} - q^2) r_d^{11}}{1 - q_0^{11}} \right) \right) (f'(1) - f'(q_0^{11})) \right. \\ & \left. \left. - \frac{1}{f'(1)} \frac{f'(1)^2 - f'(q)^2}{f'(1) - f'(q_0^{11})} + \frac{r_d^{11} - r_0^{11}}{1 - q_0^{11}} (r_d^{11} f'(1) - r_0^{11} f'(q_0^{11})) + \log \left( \frac{1 - q_0^{11}}{f'(1) - f'(q_0^{11})} \right) \right] \right\} \end{aligned} \quad (34)$$

It is possible to further extremize this expression over all the other variables but  $q_0^{11}$ , for which the saddle point conditions have a unique solution. However, the resulting expression is quite complicated and provides no insight. In practice, the complexity can be calculated in two ways. First, the extremal problem can be done numerically, initializing from  $q = 0$  where the problem reduces to that of the single-point complexity of points with energy  $E_1$  and stability  $\mu_1$ , and then taking small steps in  $q$  or other parameters to trace out the solution. This is how the data in all the plots of this paper was produced. Second, the complexity can be calculated in the near neighborhood of a reference point by expanding in small  $1 - q$ . This is what we describe in the next subsection.

#### 4.5 Expansion in the near neighborhood

If there is no overlap gap between the reference point and its nearest neighbors, their complexity can be calculated by an expansion in  $1 - q$ . First, we'll use this method to describe the most common type of stationary point in the close vicinity of a reference point. The most common neighbors of a reference point are given by further maximizing the two-point complexity over the energy  $E_1$  and stability  $\mu_1$  of the nearby points. This gives the conditions

$$\hat{\beta}_1 = 0 \qquad \mu_1 = 2r_d^{11} f''(1) \quad (35)$$

where the second is only true for  $\mu_1^2 \leq \mu_m^2$ , i.e., when the nearby points are saddle points or marginal minima. When these conditions are inserted into the complexity, an expansion is made in small  $1 - q$ , and the saddle point in the remaining parameters is taken, the result is

$$\Sigma_{12} = \frac{f'''(1)}{8f''(1)^2} (\mu_m^2 - \mu_0^2) \left( \sqrt{2 + \frac{2f''(1)(f''(1) - f'(1))}{f'''(1)f'(1)}} - 1 \right) (1 - q) + O((1 - q)^2) \quad (36)$$

independent of  $E_0$ . To describe the properties of these most common neighbors, it is convenient to first make a definition. The population of stationary points that are most common at each energy (the blue line in Fig. 2) have the relation

$$E_{\text{dom}}(\mu_0) = - \frac{f'(1)^2 + f(1)(f''(1) - f'(1))}{2f''(1)f'(1)} \mu_0 \quad (37)$$

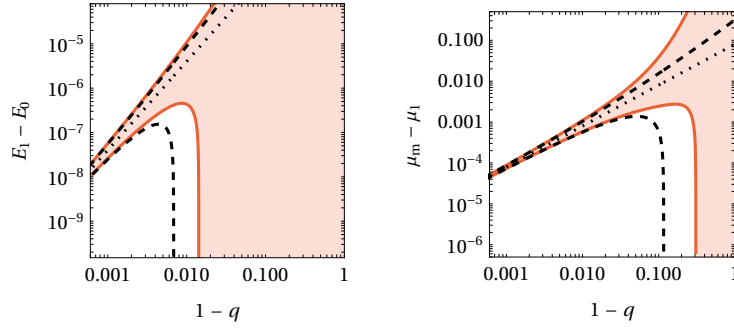


Figure 8: Demonstration of the convergence of the  $(1 - q)$ -expansion for marginal reference minima. Solid lines and shaded region show are the same as in Fig. 6 for  $E_0 - E_{\text{th}} \simeq 0.00667$ . The dotted lines show the expansion of most common neighbors, while the dashed lines in both plots show the expansion for the minimum and maximum energies and stabilities found at given  $q$ .

between  $E_0$  and  $\mu_0$  for  $\mu_0^2 \leq \mu_m^2$ . Using this definition, the energy and stability of the most common neighbors at small  $\Delta q$  are

$$E_1 = E_0 + \frac{1}{2} \frac{v_f}{u_f} (E_0 - E_{\text{dom}}(\mu_0))(1 - q)^2 + O((1 - q)^3) \quad (38)$$

$$\mu_1 = \mu_0 - \frac{v_f}{u_f} (E_0 - E_{\text{dom}}(\mu_0))(1 - q) + O((1 - q)^2) \quad (39)$$

The most common neighboring saddles to a reference saddle are much nearer to the reference in energy ( $\Delta q^2$ ) than in stability ( $\Delta q$ ). In fact, this scaling also holds for the entire range of neighbors to a reference saddle, with the limits in energy scaling like  $\Delta q^2$  and those of stability scaling like  $\Delta q$ .

Because both expressions are proportional to  $E_0 - E_{\text{dom}}(\mu_0)$ , whether the energy and stability of nearby points increases or decreases from that of the reference point depends only on whether the energy of the reference point is above or below that of the most common population at the same stability. In particular, since  $E_{\text{dom}}(\mu_m) = E_{\text{th}}$ , the threshold energy is also the pivot around which the points asymptotically nearby marginal minima change their properties.

To examine better the population of marginal points, it is necessary to look at the next term in the series of the complexity with  $\Delta q$ , since the linear coefficient becomes zero at the marginal line. This tells us something intuitive: stable minima have an effective repulsion between points, and one always finds a sufficiently small  $\Delta q$  that no stationary points are point any nearer. For the marginal minima, it is not clear that the same should be true.

When  $\mu = \mu_m$ , the linear term above vanishes. Under these conditions, the quadratic term in the expansion is

$$\Sigma_{12} = \frac{1}{2} \frac{f'''(1)v_f}{f''(1)^{3/2}u_f} \left( \sqrt{\frac{2[f'(1)(f'''(1) - f''(1)) + f''(1)^2]}{f'(1)f'''(1)}} - 1 \right) (E_0 - E_{\text{th}})(1 - q)^2 + O((1 - q)^3) \quad (40)$$

Note that this expression is only true for  $\mu = \mu_m$ . Therefore, among marginal minima, when  $E_0$  is greater than the threshold one finds neighbors at arbitrarily close distance. When  $E_0$  is less than the threshold, the complexity of nearby points is negative, and there is a desert where none are found.

The properties of the nearby states above the threshold can be further quantified. The most common points are still given by (38) and (39), but the range of available points can also be

computed, and one finds that the stability lies in the range  $\mu_1 = \mu_m + \delta\mu_1(1-q) \pm \delta\mu_2(1-q)^{3/2} + O((1-q)^2)$  where  $\delta\mu_1$  is given by the coefficient in (39) and

$$\delta\mu_2 = \frac{v_f}{f'(1)f''(1)^{3/4}} \sqrt{\frac{E_0 - E_{\text{th}}}{2} \frac{2f''(1)(f''(1) - f'(1)) + f'(1)f'''(1)}{u_f}} \quad (41)$$

Similarly, one finds that the energy lies in the range  $E_1 = E_0 + \delta E_1(1-q)^2 \pm \delta E_2(1-q)^{5/2} + O((1-q)^3)$  for  $\delta E_1$  given by the coefficient in (38) and

$$\delta E_2 = \frac{\sqrt{E_0 - E_{\text{th}}}}{4f'(1)f''(1)^{3/4}} \left( \frac{v_f}{3u_f} [f'(1)(2f''(1) - (2 - (2 - \delta q_0)\delta q_0)f'''(1)) - 2f''(1)^2] \right. \\ \left. \times [f'(1)(6f''(1) + (18 - (6 - \delta q_0)\delta q_0)f'''(1)) - 6f''(1)^2] \right)^{\frac{1}{2}} \quad (42)$$

and  $\delta q_0$  is the coefficient in the expansion  $q_0 = 1 - \delta q_0(1-q) + O((1-q)^2)$  and is given by the real root to the quintic equation

$$0 = ((16 - (6 - \delta q_0)\delta q_0)\delta q_0 - 12)f'(1)f'''(1) - 2\delta q_0(f''(1) - f'(1))f''(1) \quad (43)$$

These predictions from the small  $1-q$  expansion are compared with numeric saddle points for the complexity of marginal minima in Fig. 8, and the results agree well at small  $1-q$ .

## 5 Isolated eigenvalue

The two-point complexity depends on the spectrum at both stationary points through the determinant of their Hessians, but only on the bulk of the distribution. As we saw, this bulk is unaffected by the conditions of energy and proximity. However, these conditions give rise to small-rank perturbations to the Hessian, which can lead a subextensive number of eigenvalues leaving the bulk. We study the possibility of *one* stray eigenvalue.

We use a technique recently developed to find the smallest eigenvalue of a random matrix [21]. One defines a quadratic statistical mechanics model with configurations defined on the sphere, whose interaction tensor is given by the matrix of interest. By construction, the ground state is located in the direction of the eigenvector associated with the smallest eigenvalue, and the ground state energy is proportional to that eigenvalue.

Our matrix of interest is the Hessian evaluated at a stationary point of the mixed spherical model, conditioned on the relative position, energies, and stabilities discussed above. We must restrict the artificial spherical model to lie in the tangent plane of the ‘real’ spherical configuration space at the point of interest, to avoid our eigenvector pointing in a direction that violates the spherical constraint. A sketch of the setup is shown in Fig. 9. The free energy of this model given a point  $\mathbf{s}$  and a specific realization of the disordered Hamiltonian is

$$\beta F_H(\beta | \mathbf{s}, \omega) = -\frac{1}{N} \log \left( \int d\mathbf{x} \delta(\mathbf{x} \cdot \mathbf{s}) \delta(\|\mathbf{x}\|^2 - N) \exp \left\{ -\beta \frac{1}{2} \mathbf{x}^T \text{Hess } H(\mathbf{s}, \omega) \mathbf{x} \right\} \right) \\ = -\lim_{\ell \rightarrow 0} \frac{1}{N} \frac{\partial}{\partial \ell} \int \left[ \prod_{\alpha=1}^{\ell} d\mathbf{x}_{\alpha} \delta(\mathbf{x}_{\alpha}^T \mathbf{s}) \delta(N - \mathbf{x}_{\alpha}^T \mathbf{x}_{\alpha}) \exp \left\{ -\beta \frac{1}{2} \mathbf{x}_{\alpha}^T (\partial \partial H(\mathbf{s}) + \omega I) \mathbf{x}_{\alpha} \right\} \right] \quad (44)$$

where the first  $\delta$ -function keeps the configurations in the tangent plane, and the second enforces the spherical constraint. We have anticipated treating the logarithm with replicas. We are interested in points  $\mathbf{s}$  that have certain properties: they are stationary points of  $H$  with given energy density and



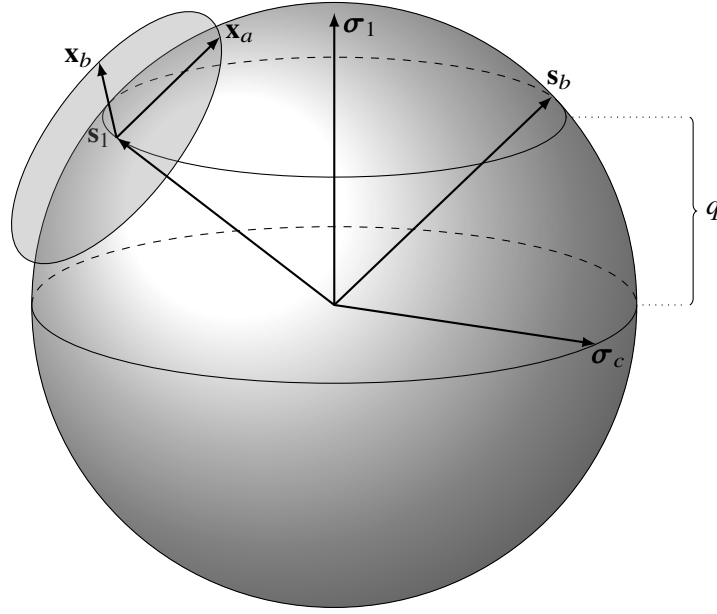


Figure 9: A sketch of the vectors involved in the calculation of the isolated eigenvalue. All replicas  $\mathbf{x}$ , which correspond with candidate eigenvectors of the Hessian evaluated at  $\mathbf{s}_1$ , sit in an  $N - 2$  sphere corresponding with the tangent plane (not to scale) of the first  $\mathbf{s}$  replica. All of the  $\mathbf{s}$  replicas lie on the sphere, constrained to be at fixed overlap  $q$  with the first of the  $\boldsymbol{\sigma}$  replicas, the reference configuration. All of the  $\boldsymbol{\sigma}$  replicas lie on the sphere.

stability, and fixed overlap from a reference configuration  $\boldsymbol{\sigma}$ . We therefore average the free energy above over such points, giving

$$\begin{aligned}
 F_H(\beta | E_1, \mu_1, q, \boldsymbol{\sigma}) &= \int \frac{d\nu_H(\mathbf{s}, \omega | E_1, \mu_1) \delta(Nq - \boldsymbol{\sigma} \cdot \mathbf{s})}{\int d\nu_H(\mathbf{s}', \omega' | E_1, \mu_1) \delta(Nq - \boldsymbol{\sigma} \cdot \mathbf{s}')} F_H(\beta | \mathbf{s}, \omega) \\
 &= \lim_{n \rightarrow 0} \int \left[ \prod_{a=1}^n d\nu_H(\mathbf{s}_a, \omega_a | E_1, \mu_1) \delta(Nq - \boldsymbol{\sigma} \cdot \mathbf{s}_a) \right] F_H(\beta | \mathbf{s}_1, \omega_1)
 \end{aligned} \tag{45}$$

again anticipating the use of replicas. Finally, the reference configuration  $\boldsymbol{\sigma}$  should itself be a stationary point of  $H$  with its own energy density and stability. Averaging over these conditions gives

$$\begin{aligned}
 F_H(\beta | E_1, \mu_1, E_2, \mu_2, q) &= \int \frac{d\nu_H(\boldsymbol{\sigma}, \boldsymbol{\varsigma} | E_0, \mu_0)}{\int d\nu_H(\boldsymbol{\sigma}', \boldsymbol{\varsigma}' | E_0, \mu_0)} F_H(\beta | E_1, \mu_1, q, \boldsymbol{\sigma}) \\
 &= \lim_{m \rightarrow 0} \int \left[ \prod_{a=1}^m d\nu_H(\boldsymbol{\sigma}_a, \boldsymbol{\varsigma}_a | E_0, \mu_0) \right] F_H(\beta | E_1, \mu_1, q, \boldsymbol{\sigma}_1)
 \end{aligned} \tag{46}$$

This formidable expression is now ready to be averaged over the disordered Hamiltonians  $H$ . Once averaged, the minimum eigenvalue of the conditioned Hessian is then given by twice the ground state energy, or

$$\lambda_{\min} = 2 \lim_{\beta \rightarrow \infty} \overline{F_H(\beta | E_1, \mu_1, E_2, \mu_2, q)} \tag{47}$$

For this calculation, there are three different sets of replicated variables. Note that, as for the computation of the complexity, the  $\boldsymbol{\sigma}_1$  and  $\mathbf{s}_1$  replicas are *special*. The first again is the only of the  $\boldsymbol{\sigma}$  replicas constrained to lie at fixed overlap with *all* the  $\mathbf{s}$  replicas, and the second is the only of the  $\mathbf{s}$  replicas at which the Hessian is evaluated.

Using the same methodology as above, the disorder-dependent terms are captured in the linear operator

$$\mathcal{O}(\mathbf{t}) = \sum_a^m \delta(\mathbf{t} - \boldsymbol{\sigma}_a) (i\hat{\boldsymbol{\sigma}}_a \cdot \partial_{\mathbf{t}} - \hat{\beta}_0) + \sum_b^n \delta(\mathbf{t} - \mathbf{s}_b) (i\hat{\mathbf{s}}_b \cdot \partial_{\mathbf{t}} - \hat{\beta}_1) - \frac{1}{2} \delta(\mathbf{t} - \mathbf{s}_1) \beta \sum_c^\ell (\mathbf{x}_c \cdot \partial_{\mathbf{t}})^2 \quad (48)$$

that is applied to  $H$  by integrating over  $\mathbf{t} \in \mathbb{R}^N$ . The resulting expression for the integrand produces dependencies only on the scalar products in (19) and on the new scalar products involving the tangent plane vectors  $\mathbf{x}$ ,

$$A_{ab} = \frac{1}{N} \mathbf{x}_a \cdot \mathbf{x}_b \quad X_{ab}^0 = \frac{1}{N} \boldsymbol{\sigma}_a \cdot \mathbf{x}_b \quad \hat{X}_{ab}^0 = -i \frac{1}{N} \hat{\boldsymbol{\sigma}}_a \cdot \mathbf{x}_b \quad X_{ab}^1 = \frac{1}{N} \mathbf{s}_a \cdot \mathbf{x}_b \quad \hat{X}_{ab}^1 = -i \frac{1}{N} \hat{\mathbf{s}}_a \cdot \mathbf{x}_b \quad (49)$$

Defining as before a block variable  $Q_x = (A, X^0, \hat{X}^0, X^1, \hat{X}^1)$  and consolidating the previous block variables  $Q = (Q_{00}, Q_{01}, Q_{11})$ , we can write the minimum eigenvalue schematically as

$$\lambda_{\min} = -2 \lim_{\beta \rightarrow \infty} \lim_{\substack{\ell \rightarrow 0 \\ m \rightarrow 0 \\ n \rightarrow 0}} \frac{\partial}{\partial \ell} \frac{1}{\beta N} \int dQ dQ_x e^{N[m\mathcal{S}_0(Q_{00}) + n\mathcal{S}(Q_{11}, Q_{01} | Q_{00}) + \ell \mathcal{S}_x(Q_x | Q_{00}, Q_{01}, Q_{11})]} \quad (50)$$

where  $\mathcal{S}_0$  is given by (21),  $\mathcal{S}$  is given by (22), and the new action  $\mathcal{S}_x$  is given by

$$\begin{aligned} \ell \mathcal{S}_x(Q_x | Q) = & -\frac{1}{2} \ell \beta \mu + \frac{1}{2} \beta \sum_b^\ell \left\{ \frac{1}{2} \beta f''(1) \sum_a^l A_{ab}^2 \right. \\ & + \sum_a^m [(\hat{\beta}_0 f''(C_{a1}^{01}) + R_{a1}^{10} f'''(C_{a1}^{01})) (X_{ab}^0)^2 + 2f''(C_{a1}^{01}) X_{ab}^0 \hat{X}_{ab}^0] \\ & \left. + \sum_a^n [(\hat{\beta}_1 f''(C_{a1}^{11}) + R_{a1}^{11} f'''(C_{a1}^{11})) (X_{ab}^1)^2 + 2f''(C_{a1}^{11}) X_{ab}^1 \hat{X}_{ab}^1] \right\} \\ & + \frac{1}{2} \log \det \left( A - \begin{bmatrix} X^0 \\ \hat{X}^0 \\ X^1 \\ \hat{X}^1 \end{bmatrix}^T \begin{bmatrix} C^{00} & iR^{00} & C^{01} & iR^{01} \\ iR^{00} & D^{00} & iR^{10} & D^{01} \\ (C^{01})^T & (iR^{10})^T & C^{11} & iR^{11} \\ (iR^{01})^T & (D^{01})^T & iR^{11} & D^{11} \end{bmatrix}^{-1} \begin{bmatrix} X^0 \\ \hat{X}^0 \\ X^1 \\ \hat{X}^1 \end{bmatrix} \right) \end{aligned} \quad (51)$$

As usual in these quenched Franz–Parisi style computations, the saddle point expressions for the variables  $Q$  in the joint limits of  $m$ ,  $n$ , and  $\ell$  to zero are independent of  $Q_x$ , and so these quantities take the same value they do for the two-point complexity that we computed above. The saddle point conditions for the variables  $Q_x$  are then fixed by extremizing with respect to the final action.

To evaluate this expression, we need a sensible ansatz for the variables  $Q_x$ . The matrix  $A$  we expect to be an ordinary hierarchical matrix, and since the model is a spherical 2-spin the finite but low temperature order will be replica symmetric with nonzero  $a_0$ . The expected form of the  $X$  matrices follows our reasoning for the 01 matrices of the previous section: namely, they should have constant rows and a column structure which matches that of the level of RSB order associated with the degrees of freedom that parameterize the columns. Since both the reference configurations and the constrained configurations have replica symmetric order, we expect

$$X^0 = \begin{array}{c} \leftarrow \ell \rightarrow \\ \begin{bmatrix} x_0 & \cdots & x_0 \\ 0 & \cdots & 0 \\ \vdots & \ddots & \vdots \\ 0 & \cdots & 0 \end{bmatrix} \begin{array}{c} \uparrow \\ m-1 \\ \downarrow \end{array} \end{array} \quad \hat{X}^0 = \begin{array}{c} \begin{bmatrix} \hat{x}_0 & \cdots & \hat{x}_0 \\ 0 & \cdots & 0 \\ \vdots & \ddots & \vdots \\ 0 & \cdots & 0 \end{bmatrix} \end{array} \quad X^1 = \begin{array}{c} \leftarrow \ell \rightarrow \\ \begin{bmatrix} 0 & \cdots & 0 \\ x_1 & \cdots & x_1 \\ \vdots & \ddots & \vdots \\ x_1 & \cdots & x_1 \end{bmatrix} \begin{array}{c} \uparrow \\ n-1 \\ \downarrow \end{array} \end{array} \quad \hat{X}^1 = \begin{array}{c} \begin{bmatrix} \hat{x}_1^0 & \cdots & \hat{x}_1^0 \\ \hat{x}_1^1 & \cdots & \hat{x}_1^1 \\ \vdots & \ddots & \vdots \\ \hat{x}_1^1 & \cdots & \hat{x}_1^1 \end{bmatrix} \end{array} \quad (52)$$

Here, the lower block of the 0 matrices is zero, because these replicas have no overlap with the reference or anything else. The first row of the  $X^1$  matrix needs to be zero because of the constraint that the tangent space vectors lie in the tangent plane to the sphere, and therefore have  $\mathbf{x}_a \cdot \mathbf{s}_1 = 0$  for any  $a$ . This produces five parameters to deal with, which we compile in the vector  $\mathcal{X} = (x_0, \hat{x}_0, x_1, \hat{x}_1^1, \hat{x}_1^0)$ .

Inserting this ansatz is straightforward in the first part of (51), but the term with log det is more complicated. We must invert the block matrix inside. We define

$$\begin{bmatrix} C^{00} & iR^{00} & C^{01} & iR^{01} \\ iR^{00} & D^{00} & iR^{10} & D^{01} \\ (C^{01})^T & (iR^{10})^T & C^{11} & iR^{11} \\ (iR^{01})^T & (D^{10})^T & iR^{11} & D^{11} \end{bmatrix}^{-1} = \begin{bmatrix} M_{11} & M_{12} \\ M_{12}^T & M_{22} \end{bmatrix} \quad (53)$$

where the blocks inside the inverse are given by

$$M_{11} = \left( \begin{bmatrix} C^{00} & iR^{00} \\ iR^{00} & D^{00} \end{bmatrix} - \begin{bmatrix} C^{01} & iR^{01} \\ iR^{10} & D^{01} \end{bmatrix} \begin{bmatrix} C^{11} & iR^{11} \\ iR^{11} & D^{11} \end{bmatrix}^{-1} \begin{bmatrix} C^{01} & iR^{01} \\ iR^{10} & D^{01} \end{bmatrix}^T \right)^{-1} \quad (54)$$

$$M_{12} = -M_{11} \begin{bmatrix} C^{01} & iR^{01} \\ iR^{10} & D^{01} \end{bmatrix} \begin{bmatrix} C^{11} & iR^{11} \\ iR^{11} & D^{11} \end{bmatrix}^{-1} \quad (55)$$

$$M_{22} = \left( \begin{bmatrix} C^{11} & iR^{11} \\ iR^{11} & D^{11} \end{bmatrix} - \begin{bmatrix} C^{01} & iR^{01} \\ iR^{10} & D^{01} \end{bmatrix}^T \begin{bmatrix} C^{00} & iR^{00} \\ iR^{00} & D^{00} \end{bmatrix}^{-1} \begin{bmatrix} C^{01} & iR^{01} \\ iR^{10} & D^{01} \end{bmatrix} \right)^{-1} \quad (56)$$

Here,  $M_{22}$  is the inverse of the matrix already analyzed as part of (22). Following our discussion of the inverses of block replica matrices above, and reasoning about their products with the rectangular block constant matrices, things can be worked out from here. For instance, the second term in  $M_{11}$  contributes nothing once the appropriate limits are taken, because each contribution is proportional to  $n$ .

The contribution can be written as

$$\begin{bmatrix} X_0 \\ i\hat{X}_0 \end{bmatrix}^T M_{11} \begin{bmatrix} X_0 \\ i\hat{X}_0 \end{bmatrix} + 2 \begin{bmatrix} X_0 \\ i\hat{X}_0 \end{bmatrix}^T M_{12} \begin{bmatrix} X_1 \\ i\hat{X}_1 \end{bmatrix} + \begin{bmatrix} X_1 \\ i\hat{X}_1 \end{bmatrix}^T M_{22} \begin{bmatrix} X_1 \\ i\hat{X}_1 \end{bmatrix} \quad (57)$$

and without too much reasoning one can see that the result is an  $\ell \times \ell$  constant matrix. If  $A$  is a replica matrix and  $c$  is a constant, then

$$\log \det(A - c) = \log \det A - \frac{c}{\sum_{i=0}^k (a_{i+1} - a_i) x_{i+1}} \quad (58)$$

where  $a_{k+1} = 1$  and  $x_{k+1} = 1$ . The basic form of the action is (for replica symmetric  $A$ )

$$2\mathcal{S}_x(Q_x | Q) = -\beta\mu + \frac{1}{2}\beta^2 f''(1)(1 - a_0^2) + \log(1 - a_0) + \frac{a_0}{1 - a_0} + \mathcal{X}^T \left( \beta B - \frac{1}{1 - a_0} C \right) \mathcal{X} \quad (59)$$

where the matrix  $B$  comes from the  $\mathcal{X}$ -dependent parts of the first lines of (51) and is given by

$$B = \begin{bmatrix} \hat{\beta}_0 f''(q) + r_{10} f'''(q) & f''(q) & 0 & 0 & 0 \\ f''(q) & 0 & 0 & 0 & 0 \\ 0 & 0 & -\hat{\beta}_1 f''(q_0^{11}) - r_0^{11} f'''(q_0^{11}) & -f''(q_0^{11}) & 0 \\ 0 & 0 & -f''(q_0^{11}) & 0 & 0 \\ 0 & 0 & 0 & 0 & 0 \end{bmatrix} \quad (60)$$

and where the matrix  $C$  encodes the coefficients of the quadratic form (57), and is given element-wise by

$$\begin{aligned}
C_{11} &= d_d^{00} f'(1) & C_{12} &= r_d^{00} f'(1) & C_{22} &= -f'(1) \\
C_{13} &= \frac{1}{1-q_0} \left( (r_d^{11} - r_0^{11}) \left( r^{01} - q \frac{r_d^{11} - r_0^{11}}{1-q_0} \right) (f'(1) - f'(q_0)) + q f'(1) d_d^{00} + r_d^{00} (r^{10} f'(1) + (r_d^{11} - r_0^{11}) f'(q)) \right) \\
C_{15} &= r_d^{00} f'(q) + \left( r^{01} - q \frac{r_d^{11} - r_0^{11}}{1-q_0} \right) (f'(1) - f'(q_0)) & C_{14} &= -C_{15} \\
C_{23} &= \frac{1}{1-q_0} \left( (q r_d^{00} - r^{10}) f'(1) - (r_d^{11} - r_0^{11}) f'(q) \right) & C_{24} &= f'(q) & C_{25} &= -C_{24} \\
C_{33} &= -\frac{r_d^{11} - r_0^{11}}{1-q_0} \left[ \frac{r_d^{11} - r_0^{11}}{1-q_0} f'(1) - 2 \left( \frac{q r^{01} - r_0^{11}}{1-q_0} + \frac{1-q^2}{1-q_0} \frac{r_d^{11} - r_0^{11}}{1-q_0} \right) (f'(1) - f'(q_0)) - 2 \frac{q r^{00} - r^{10}}{1-q_0} f'(q) \right] \\
&\quad - \frac{1-q^2}{(1-q_0)^2} - \frac{(r^{10} - q r_d^{00})^2}{(1-q_0)^2} f'(1) \\
C_{34} &= -(q r^{01} - r_0^{11}) \frac{f'(1) - f'(q_0)}{1-q_0} - \frac{r_d^{11} - r_0^{11}}{1-q_0} \left( \frac{1-q^2}{1-q_0} (f'(1) - f'(q_0)) - f'(q_0) \right) - f'(q) \frac{q r_d^{00} - r^{10}}{1-q_0} \\
C_{35} &= -C_{34} - \frac{r_d^{11} - r_0^{11}}{1-q_0} (f'(1) - f'(q_0)) & C_{44} &= f'(1) - 2f'(q_0) & C_{45} &= f'(q_0) & C_{55} &= -f'(1)
\end{aligned} \tag{61}$$

The saddle point conditions read

$$0 = -\beta^2 f''(1) a_0 + \frac{a_0 - \mathcal{X}^T C \mathcal{X}}{(1-a_0)^2} \quad 0 = \left( \beta B - \frac{1}{1-a_0} C \right) \mathcal{X} \tag{62}$$

Note that the second of these conditions implies that the quadratic form in  $\mathcal{X}$  in the action vanishes at the saddle.

We would like to take the limit of  $\beta \rightarrow \infty$ . As is usual in the two-spin model, the appropriate limit of the order parameter is  $a_0 = 1 - (y\beta)^{-1}$ . Upon inserting this scaling and taking the limit, we finally find

$$\lambda_{\min} = -2 \lim_{\beta \rightarrow \infty} \frac{1}{\beta} \mathcal{S}_x = \mu - \left( y + \frac{1}{y} f''(1) \right) \tag{63}$$

with associated saddle point conditions

$$0 = -f''(1) + y^2 (1 - \mathcal{X}^T C \mathcal{X}) \quad 0 = (B - yC) \mathcal{X} \tag{64}$$

The trivial solution, which gives the bottom of the semicircle, is for  $\mathcal{X} = 0$ . When this is satisfied, the first equation gives  $y^2 = f''(1)$ , and

$$\lambda_{\min} = \mu - \sqrt{4f''(1)} = \mu - \mu_m \tag{65}$$

as expected. The nontrivial solutions have nonzero  $\mathcal{X}$ . The only way to satisfy this with the saddle conditions is for  $y$  such that one of the eigenvalues of  $B - yC$  is zero. In this case, if the normalized eigenvector associated with the zero eigenvalue is  $\hat{\mathcal{X}}_0$ ,  $\mathcal{X} = \|\mathcal{X}_0\| \hat{\mathcal{X}}_0$  is a solution. The magnitude of the solution is set by the other saddle point condition, namely

$$\|\mathcal{X}_0\|^2 = \frac{1}{\hat{\mathcal{X}}_0^T C \hat{\mathcal{X}}_0} \left( 1 - \frac{f''(1)}{y^2} \right) \tag{66}$$

In practice, we find that  $\hat{\mathcal{X}}_0^T C \hat{\mathcal{X}}_0$  is positive at the saddle point. Therefore, for the solution to make sense we must have  $y^2 \geq f''(1)$ . In practice, there is at most *one*  $y$  which produces a zero eigenvalue of  $B - yC$  and satisfies this inequality, so the solution seems to be unique.

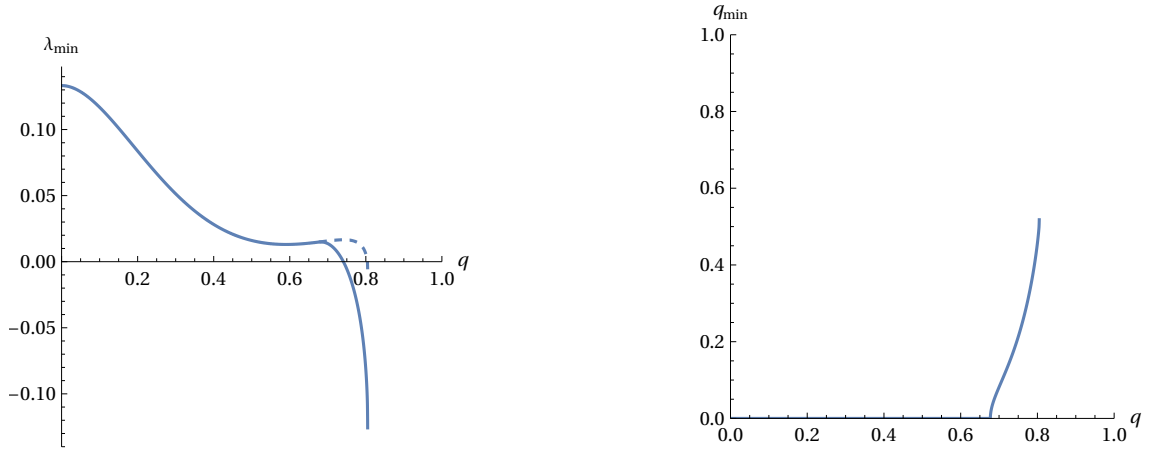


Figure 10: Properties of the isolated eigenvalue and the overlap of its associated eigenvector with the direction of the reference point. These curves correspond with the lower solid curve in Fig. 3. **Left:** The value of the minimum eigenvalue as a function of overlap. The dashed line shows the continuation of the bottom of the semicircle. Where the dashed line separates from the solid line, the isolated eigenvalue has appeared. **Right:** The overlap between the eigenvector associated with the minimum eigenvalue and the direction of the reference point. The overlap is zero until an isolated eigenvalue appears, and then it grows continuously until the nearest neighbor is reached.

In this solution, we simultaneously find the smallest eigenvalue and information about the orientation of its associated eigenvector: namely, its overlap with the tangent vector that points directly toward the reference spin. This is directly related to  $x_0$ . This tangent vector is  $\mathbf{x}_{0\leftarrow 1} = \frac{1}{1-q}(\boldsymbol{\sigma}_0 - q\mathbf{s}_a)$ , which is normalized and lies strictly in the tangent plane of  $\mathbf{s}_a$ . Then

$$q_{\min} = \frac{\mathbf{x}_{0\leftarrow 1} \cdot \mathbf{x}_{\min}}{N} = \frac{x_0}{1-q} \quad (67)$$

The emergence of an isolated eigenvalue and its associated eigenvector are shown in Fig. 10, for the same reference point properties as in Fig. 3.

## 6 Franz–Parisi potential

Here, we compute the Franz–Parisi potential for this model at zero temperature, with respect to a reference configuration fixed to be a stationary point of energy  $E_0$  and stability  $\mu_0$  as before [22, 23]. The potential is defined as the average free energy of a system constrained to lie with a fixed overlap  $q$  with a reference configuration (here a stationary point with fixed energy and stability), and given by

$$\beta V_{\beta}(q | E_0, \mu_0) = -\frac{1}{N} \int \frac{d\nu_H(\boldsymbol{\sigma}, \boldsymbol{\zeta} | E_0, \mu_0)}{\int d\nu_H(\boldsymbol{\sigma}', \boldsymbol{\zeta}' | E_0, \mu_0)} \log \left( \int ds \delta(\|s\|^2 - N) \delta(\boldsymbol{\sigma} \cdot \mathbf{s} - Nq) e^{-\beta H(\mathbf{s})} \right) \quad (68)$$

Both the denominator and the logarithm are treated using the replica trick, which yields

$$\beta V_{\beta}(q | E_0, \mu_0) = -\frac{1}{N} \lim_{n \rightarrow 0} \frac{\partial}{\partial n} \int \left( \prod_{b=1}^m d\nu_H(\boldsymbol{\sigma}_b, \boldsymbol{\zeta}_b | E_0, \mu_0) \right) \left( \prod_{a=1}^n ds_a \delta(\|s_a\|^2 - N) \delta(\boldsymbol{\sigma}_1 \cdot \mathbf{s}_a - Nq) e^{-\beta H(\mathbf{s}_a)} \right) \quad (69)$$

The derivation of this proceeds in much the same way as for the complexity or the isolated eigenvalue. Once the  $\delta$ -functions are converted to exponentials, the  $H$ -dependent terms can be expressed by convolution with the linear operator

$$O(\mathbf{t}) = \sum_a^m \delta(\mathbf{t} - \boldsymbol{\sigma}_a) (i\hat{\boldsymbol{\sigma}}_a \cdot \partial_{\mathbf{t}} - \hat{\beta}_0) - \beta \sum_a^n \delta(\mathbf{t} - \mathbf{s}_a) \quad (70)$$

Averaging over  $H$  squares the application of this operator to  $f$  as before. After performing a Hubbard–Stratonovich using matrix order parameters identical to those used in the calculation of the complexity, we find that

$$\beta V_{\beta}(q | E_0, \mu_0) = -\frac{1}{N} \lim_{\substack{m \rightarrow 0 \\ n \rightarrow 0}} \frac{\partial}{\partial n} \int dQ_0 dQ_1 e^{Nm\mathcal{S}_0(Q_0) + Nn\mathcal{S}_{\text{FP}}(Q_1 | Q_0)} \quad (71)$$

where  $\mathcal{S}_0$  is the same as in (21) and

$$n\mathcal{S}_{\text{FP}} = \frac{1}{2}\beta^2 \sum_{ab}^n f(Q_{ab}) + \beta \sum_a^m \sum_b^n [\hat{\beta}_0 f(C_{ab}^{01}) + R_{ab}^{10} f'(C_{ab}^{01})] + \frac{1}{2} \log \det \left( Q - \begin{bmatrix} C^{01} \\ iR^{10} \end{bmatrix}^T \begin{bmatrix} C^{00} & iR^{00} \\ iR^{00} & D^{00} \end{bmatrix}^{-1} \begin{bmatrix} C^{01} \\ iR^{10} \end{bmatrix} \right) \quad (72)$$

Here, because we are at low but nonzero temperature for the constrained configuration, we make a 1RSB ansatz for the matrix  $Q$ , while the 00 matrices will take their saddle point value for the one-point complexity and the 01 matrices have the same structure as (27). Inserting these gives

$$\begin{aligned} \beta V_{\beta} = & \frac{1}{2}\beta^2 [f(1) - (1-x)f(q_1) - xf(q_0)] + \beta\hat{\beta}_0 f(q) + \beta r^{10} f'(q) - \frac{1-x}{x} \log(1-q_1) \\ & + \frac{1}{x} \log(1 - (1-x)q_1 - xq_0) + \frac{q_0 - d_d^{00} f'(1)q^2 - 2r_d^{00} f'(1)r^{10}q + (r^{10})^2 f'(1)}{1 - (1-x)q_1 - xq_0} \end{aligned} \quad (73)$$

The saddle point for  $r^{10}$  can be taken explicitly. After this, we take the limit of  $\beta \rightarrow \infty$ . There are two possibilities. First, in the replica symmetric case  $x = 1$ , and in the limit of large  $\beta$   $q_0$  will scale like  $q_0 = 1 - (y_0\beta)^{-1}$ . Inserting this, the limit is

$$V_{\infty}^{\text{RS}} = -\hat{\beta}_0 f(q) - r_d^{00} f'(q)q - \frac{1}{2} \left( y_0(1-q^2) + \frac{f'(1)^2 - f'(q)^2}{y_0 f'(1)} \right) \quad (74)$$

The saddle point in  $y_0$  can now be taken, taking care to choose the solution for  $y_0 > 0$ . This gives

$$V_{\infty}^{\text{RS}}(q | E_0, \mu_0) = -\hat{\beta}_0 f(q) - r_d^{00} f'(q)q - \sqrt{(1-q^2) \left( 1 - \frac{f'(q)^2}{f'(1)^2} \right)} \quad (75)$$

The second case is when the inner statistical mechanics problem has replica symmetry breaking. Here,  $q_0$  approaches a nontrivial limit, but  $x = z\beta^{-1}$  approaches zero and  $q_1 = 1 - (y_1\beta)^{-1}$  approaches one. The result is

$$\begin{aligned} V_{\infty}^{\text{1RSB}}(q | E_0, \mu_0) = & -\hat{\beta}_0 f(q) - r_d^{00} f'(q)q - \frac{1}{2} \left( z(f(1) - f(q_0)) + \frac{f'(1)}{y_1} - \frac{y_1(q^2 - q_0)}{1 + y_1 z(1 - q_0)} \right. \\ & \left. - (1 + y_1 z(1 - q_0)) \frac{f'(q)^2}{y_1 f'(1)} + \frac{1}{z} \log(1 + zy_1(1 - q_0)) \right) \end{aligned} \quad (76)$$

Though the saddle point in  $y_1$  can be evaluated in this expression, it delivers no insight. The final potential is found by taking the saddle over  $z$ ,  $y_1$ , and  $q_0$ . A plot comparing the result to the minimum energy saddles is found in Fig. 4. As noted above, there is little qualitatively different from what was found in [9] for the pure models.

## 7 Conclusion

We have computed the complexity of neighboring stationary points for the mixed spherical models. When we studied the neighborhoods of marginal minima, we found something striking: only those at the threshold energy have other marginal minima nearby. For the many marginal minima away from the threshold (including the exponential majority), there is a gap in overlap between them.

This has implications for pictures of relaxation and aging. In most  $p + s$  models studied, quenches from infinite to zero temperature (gradient descent starting from a random point) relax towards marginal states with energies above the threshold energy [15], while at least in some models a quench to zero temperature from a temperature around the dynamic transition relaxes towards marginal states with energies below the threshold energy [7, 8]. We found (see especially Figs. 5 and 6) that the neighborhoods of marginal states above and below the threshold are quite different, and yet the emergent aging behaviors relaxing toward states above and below the threshold seem to be the same. Therefore, this kind of dynamics appears to be insensitive to the neighborhood of the marginal state being approached. To understand something better about why certain states attract the dynamics in certain situations, nonlocal information, like the structure of their entire basin of attraction, seems vital.

It is possible that replica symmetry breaking among the constrained stationary points could change the details of the two-point complexity of very nearby states. Indeed, it is difficult to rule out RSB in complexity calculations. However, such corrections would not change the overarching conclusions of this paper, namely that most marginal minima are separated from each other by a macroscopic overlap gap and high barriers. This is because the replica symmetric complexity bounds any RSB complexities from above, and so RSB corrections can only decrease the complexity. Therefore, the overlap gaps, which correspond to regions of negative complexity, cannot be removed by a more detailed saddle point ansatz.

Our calculation studied the neighborhood of typical reference points with the given energy and stability. However, it is possible that marginal minima with atypical neighborhoods actually attract the dynamics. To determine this, a different type of calculation is needed. As our calculation is akin to the quenched Franz–Parisi potential, study of atypical neighborhoods would entail something like the annealed Franz–Parisi approach, i.e.,

$$\Sigma^*(E_0, \mu_0, E_1, \mu_1, q) = \frac{1}{N} \log \left( \int d\nu_H(\boldsymbol{\sigma}, \boldsymbol{\zeta} \mid E_0, \mu_0) d\nu_H(\mathbf{s}, \boldsymbol{\omega} \mid E_1, \mu_1) \delta(Nq - \boldsymbol{\sigma} \cdot \mathbf{s}) \right) \quad (77)$$

which puts the two points on equal footing. This calculation and exploration of the atypical neighborhoods it reveals is a clear future direction.

The methods developed in this paper are straightforwardly (if not easily) generalized to landscapes with replica symmetry broken complexities [24]. We suspect that many of the qualitative features of this study would persist, with neighboring states being divided into different clusters based on the RSB order but with the basic presence or absence of overlap gaps and the nature of the stability of near-neighbors remaining unchanged. Interesting structure might emerge in the arrangement of marginal states in FRSB systems, where the ground state itself is marginal and coincides with the threshold.

**Acknowledgements** The author would like to thank Valentina Ros, Giampaolo Folena, Chiara Cammarota, and Jorge Kurchan for useful discussions related to this work.

**Funding information** JK-D is supported by a DYN SYS MATH Specific Initiative by the INFN.

## References

- [1] A. Cavagna, *Fragile vs. strong liquids: A saddles-ruled scenario*, Europhysics Letters (EPL) **53**(4), 490 (2001), doi:[10.1209/epl/i2001-00179-4](https://doi.org/10.1209/epl/i2001-00179-4).
- [2] F. H. Stillinger and P. G. Debenedetti, *Glass transition thermodynamics and kinetics*, Annual Review of Condensed Matter Physics **4**(1), 263 (2013), doi:[10.1146/annurev-conmatphys-030212-184329](https://doi.org/10.1146/annurev-conmatphys-030212-184329).
- [3] T. R. Kirkpatrick and D. Thirumalai, *Colloquium: Random first order transition theory concepts in biology and physics*, Reviews of Modern Physics **87**(1), 183 (2015), doi:[10.1103/revmodphys.87.183](https://doi.org/10.1103/revmodphys.87.183).
- [4] T. Castellani and A. Cavagna, *Spin-glass theory for pedestrians*, Journal of Statistical Mechanics: Theory and Experiment **2005**(05), P05012 (2005), doi:[10.1088/1742-5468/2005/05/p05012](https://doi.org/10.1088/1742-5468/2005/05/p05012).
- [5] G. Biroli, *Dynamical TAP approach to mean field glassy systems*, Journal of Physics A: Mathematical and General **32**(48), 8365 (1999), doi:[10.1088/0305-4470/32/48/301](https://doi.org/10.1088/0305-4470/32/48/301).
- [6] M. Sellke, *The threshold energy of low temperature Langevin dynamics for pure spherical spin glasses* (2023), [2305.07956v1](https://arxiv.org/abs/2305.07956).
- [7] G. Folena, S. Franz and F. Ricci-Tersenghi, *Rethinking mean-field glassy dynamics and its relation with the energy landscape: The surprising case of the spherical mixed  $p$ -spin model*, Physical Review X **10**, 031045 (2020), doi:[10.1103/PhysRevX.10.031045](https://doi.org/10.1103/PhysRevX.10.031045).
- [8] G. Folena, S. Franz and F. Ricci-Tersenghi, *Gradient descent dynamics in the mixed  $p$ -spin spherical model: finite-size simulations and comparison with mean-field integration*, Journal of Statistical Mechanics: Theory and Experiment **2021**(3), 033302 (2021), doi:[10.1088/1742-5468/abe29f](https://doi.org/10.1088/1742-5468/abe29f).
- [9] V. Ros, G. Biroli and C. Cammarota, *Complexity of energy barriers in mean-field glassy systems*, EPL (Europhysics Letters) **126**(2), 20003 (2019), doi:[10.1209/0295-5075/126/20003](https://doi.org/10.1209/0295-5075/126/20003).
- [10] J. Kurchan and L. Laloux, *Phase space geometry and slow dynamics*, Journal of Physics A: Mathematical and General **29**(9), 1929 (1996), doi:[10.1088/0305-4470/29/9/009](https://doi.org/10.1088/0305-4470/29/9/009).
- [11] T. R. Kirkpatrick and D. Thirumalai,  *$p$ -spin-interaction spin-glass models: Connections with the structural glass problem*, Physical Review B **36**(10), 5388 (1987), doi:[10.1103/physrevb.36.5388](https://doi.org/10.1103/physrevb.36.5388).
- [12] A. Crisanti and H.-J. Sommers, *The spherical  $p$ -spin interaction spin glass model: the statics*, Zeitschrift für Physik B Condensed Matter **87**(3), 341 (1992), doi:[10.1007/bf01309287](https://doi.org/10.1007/bf01309287).
- [13] A. Crisanti and L. Leuzzi, *Spherical  $2 + p$  spin-glass model: An exactly solvable model for glass to spin-glass transition*, Physical Review Letters **93**(21), 217203 (2004), doi:[10.1103/physrevlett.93.217203](https://doi.org/10.1103/physrevlett.93.217203).
- [14] G. Ben Arous, E. Subag and O. Zeitouni, *Geometry and temperature chaos in mixed spherical spin glasses at low temperature: The perturbative regime*, Communications on Pure and Applied Mathematics **73**(8), 1732 (2019), doi:[10.1002/cpa.21875](https://doi.org/10.1002/cpa.21875).
- [15] G. Folena and F. Zamponi, *On weak ergodicity breaking in mean-field spin glasses* (2023), [2303.00026v2](https://arxiv.org/abs/2303.00026).



- [16] M. Kac, *On the average number of real roots of a random algebraic equation*, Bulletin of the American Mathematical Society **49**(4), 314 (1943).
- [17] S. O. Rice, *Mathematical analysis of random noise*, Bell System Technical Journal **23**(3), 282 (1944), doi:[10.1002/j.1538-7305.1944.tb00874.x](https://doi.org/10.1002/j.1538-7305.1944.tb00874.x).
- [18] A. Cavagna, I. Giardinà and G. Parisi, *Stationary points of the Thouless-Anderson-Palmer free energy*, Physical Review B **57**(18), 11251 (1998), doi:[10.1103/physrevb.57.11251](https://doi.org/10.1103/physrevb.57.11251).
- [19] Y. V. Fyodorov, H.-J. Sommers and I. Williams, *Density of stationary points in a high dimensional random energy landscape and the onset of glassy behavior*, JETP Letters **85**(5), 261 (2007), doi:[10.1134/s0021364007050098](https://doi.org/10.1134/s0021364007050098).
- [20] A. J. Bray and D. S. Dean, *Statistics of critical points of Gaussian fields on large-dimensional spaces*, Physical Review Letters **98**(15), 150201 (2007), doi:[10.1103/physrevlett.98.150201](https://doi.org/10.1103/physrevlett.98.150201).
- [21] H. Ikeda, *Bose–einstein-like condensation of deformed random matrix: a replica approach*, Journal of Statistical Mechanics: Theory and Experiment **2023**(2), 023302 (2023), doi:[10.1088/1742-5468/acb7d6](https://doi.org/10.1088/1742-5468/acb7d6).
- [22] S. Franz and G. Parisi, *Recipes for metastable states in spin glasses*, Journal de Physique I **5**(11), 1401 (1995), doi:[10.1051/jp1:1995201](https://doi.org/10.1051/jp1:1995201).
- [23] S. Franz and G. Parisi, *Effective potential in glassy systems: theory and simulations*, Physica A: Statistical Mechanics and its Applications **261**(3-4), 317 (1998), doi:[10.1016/s0378-4371\(98\)00315-x](https://doi.org/10.1016/s0378-4371(98)00315-x).
- [24] J. Kent-Dobias and J. Kurchan, *How to count in hierarchical landscapes: a full solution to mean-field complexity*, Physical Review E **107**(6), 064111 (2023), doi:[10.1103/PhysRevE.107.064111](https://doi.org/10.1103/PhysRevE.107.064111).